Energy transfer from Cr to Nd in substitutional crystal $Y_3Ga_xAl_{5-x}O_{12}$ codoped with Nd and Cr

Kazuki Takagi [a], Mitsuo Yamaga [a,*], Encarnacion G. Villora [b], Kiyoshi Shimamura [b], Kazuo Hasegawa [c], Hiroshi Ito [c], Shintaro Mizuno [c], Yasuhiko Takeda [c], Thomas P. J. Han [d]

[a] Department of Mathematical and Design Engineering, Gifu University, Gifu 501-1193, Japan

[b] National Institute for Materials Science, Tsukuba 305-0044, Japan

[c] Toyota Central R&D Laboratories, Nagakute 480-1192, Japan

[d] Department of Physics, University of Strathclyde, Glasgow G4 0NG, Scotland, United Kingdom

Keywords : Neodymium, Chromium, substitutional garnet crystal, Inhomogeneous broadening, Energy transfer

*Corresponding author: Tel.:+81 58 2933052; fax:+81 58 2932415.

E-mail address: yamaga@gifu-u.ac.jp (M. Yamaga)

ABSTRACT

Garnet crystals codoped with Nd^{3+} and Cr^{3+} ions are a candidate for solar-pumped laser materials. Substitutional disordered crystals $Y_3Ga_xAl_{5-x}O_{12}$ were prepared to improve the pumping efficiency of Nd^{3+} luminescence and energy transfer from Cr^{3+} to Nd^{3+} ions. The substitutional disordered crystal host produced inhomogeneous broadening of the Nd^{3+} and Cr^{3+} optical spectra. Enhancement of overlapping between the Cr^{3+} absorption bands and the solar spectrum, and between the Cr^{3+} luminescence bands and the Nd^{3+} absorption lines led to the increases of the pumping efficiency and the energy transfer rates, respectively. The excitation spectrum of the Nd^{3+} luminescence, the nonexponential decay curves of the Cr^{3+} luminescence, and the quantum yields of the Cr^{3+} and Nd^{3+} luminescence have given evidence on the energy transfer from Cr^{3+} to Nd^{3+} ions.

1. Introduction

Neodymium ions doped yttrium aluminum garnet $Y_3Al_5O_{12}$ (Nd:YAG) single crystal is one of the most commercially successful solid-state laser materials [1]. The Nd^{3+} absorption spectrum of Nd:YAG consists of weak and narrow lines in the ultraviolet (UV), visible and near infrared (IR) ranges because of the parity-forbidden transitions between the intra $4f^3$ multiplets of Nd^{3+} ions. The use of a sensitizer is necessary in order to enhance the efficiency of solar or flash lamp excitation/pump lanthanide laser systems. Cr^{3+} ion is one of the best sensitizers because its absorption spectrum is composed of two intense and broad bands in the visible range from 400 to 700 nm [2]. The energy transfer from Cr^{3+} to Nd^{3+} strongly depends on overlapping between the Cr^{3+} luminescence and the Nd^{3+} absorption spectra [3]. As the $^4T_2$ excited state of Cr^{3+} in Nd:Cr:YAG lies about 1000 cm^{-1} above the lowest ^2E excited state, the contribution of the $^4T_2$ excited state to the energy transfer is dominant at high temperatures up to about 400 K [2].

Since 1980s, the garnet family has extended greatly, including the well-studied gadolinium scandium gallium garnet codoped with Nd^{3+} and Cr^{3+} ions (Nd:Cr:GSGG) [4-6]. As the energy separation between the lowest ^2E and the higher $^4T_2$ excited states of the Cr^{3+} ions in Nd:Cr:GSGG is about 100 cm^{-1}, the energy transfer from Cr^{3+} to Nd^{3+} via the $^4T_2$ excited state occurs efficiently even at low temperatures [4], compared with that in Nd:Cr:YAG [2]. However, the poor thermal conductivity of the GSGG material prevents further commercial development of this material [1].

Substitution of dopant ions for lattice ions causes structural and chemical defects. These lattice defects lead to reduction of quantum yield of laser materials, whilst internal strains adversely affect laser operation. The distribution of defects and strains produces inhomogeneous broadening of the spectral transition lines [3]. An example of the latter effect is the substitutional disordered crystals, $Y_3Ga_xAl_{5-x}O_{12}$, doped with Nd^{3+} ions, where Ga^{3+} preferentially substitutes for Al^{3+} occupying an octahedral site [3,7]. As a consequence, the main peaks of the Nd^{3+} transition lines are blue-shifted when x increased. The line-widths are at their maximum for the $x = 2.5$ composition [3,7].

In this paper, such substitutional disorder system is applied to the garnet crystals $Y_3Ga_xAl_{5-x}O_{12}$ codoped with Nd^{3+} and Cr^{3+} ions. As the ionic radius of Ga^{3+} is larger than that of Al^{3+}, the octahedral crystal field of Cr^{3+} is expected to be weak. Hence, the substitution of Ga^{3+} for Al^{3+} induces not only inhomogeneous broadening of the Cr^{3+} and Nd^{3+} absorption/luminescence

spectra, but also a decrease of the energy separation between the lowest ^2E and the higher $^4T_2$ excited states of the Cr^{3+} ion. This reduction of the separation energy leads to thermal population to the higher $^4T_2$ excited states at room temperature, so enhancing the energy transfer process from Cr^{3+} to Nd^{3+}.

2. Experimental procedure

Substitutional yttrium gallium aluminum garnet crystals codoped with neodymium and chromium ions (Nd:Cr:YGAG) were grown by the Czochralski method. A [111] oriented YAG single crystal was used as seed. High-purity oxide powders, Y_2O_3 (99.99 %), Ga_2O_3 (99.99 %), Al_2O_3 (99.99 %), were used as starting materials. Y_2O_3, Ga_2O_3, and Al_2O_3 powders were weighed and mixed at a molar ratio of 3 : 1 : 4. Impurity concentrations of Nd_2O_3 and Cr_2O_3 were 1 molar % and 2.5 molar % to Y_2O_3 and Ga_2O_3/Al_2O_3, respectively. The composition of the as-grown crystal was estimated to be $Y_{2.97}Nd_{0.02}Ga_{0.22}Al_{4.68}Cr_{0.11}O_{12}$ by the inductively coupled plasma (ICP) method. The concentrations of Cr^{3+} and Nd^{3+} ions to Al^{3+}/Ga^{3+} and Y^{3+} ions are estimated to be 2.2% and 0.67%, respectively.

YAG ceramics codoped with 1% Nd and 1% Cr (Nd:Cr:YAG), and YAG single crystals doped with 1% Cr (Cr:YAG) or 1% Nd (Nd:YAG) were used in this study as comparison with the Nd:Cr:YGAG crystal [8].

Optical absorption spectra were measured using a Perkin Elmer Lambda950 spectrophotometer at room temperature. Luminescence and excitation spectra were measured using a JASCO FP800 spectrofluorometer at room temperature. Temperature dependence of luminescence spectra in the range of 8-300 K was measured using the UVSOR facility in the Institute of Molecular Science at Okazaki, Japan. Decay curves of luminescence were measured using a Hamamatsu Photonics Quantaurus-Tau C11367 spectrometer, where sample temperatures from 2 to 300 K were achieved using an Oxford Opticool SRDK-101D. Quantum yields of luminescence were measured using a Hamamatsu Photonics Quantaurus-QY C11347 spectrometer at room temperature.

3. Experimental results

Figure 1 shows the optical absorption spectrum of Nd:Cr:YGAG in comparison with that of Nd:Cr:YAG at 300 K. The baseline for the Nd:Cr:YGAG spectrum is shifted for clarity. The sharp lines observed in the UV, visible, and near IR ranges for Nd:Cr:YGAG and Nd:Cr:YAG are due to the optical transitions from the $^4I_{9/2}$ ground state multiplet of the Nd^{3+} ion to the excited states multiplets [2,3,8]. Three broad bands with peaks at 270, 430, and 600 nm are assigned to the optical transitions from the $^4A_2$ ground state of the Cr^{3+} ion to the $^4T_1(2)$, $^4T_1(1)$, and $^4T_2$ excited states, respectively [2,3,8]. The absorption coefficients of the two Cr^{3+} bands and the Nd^{3+} lines in the range of 740-900 nm for Nd:Cr:YGAG are ~2.5 and ~0.7 times larger than those in Nd:Cr:YAG. These estimated ratios are nearly equal to the concentration ratios, 2.2 and 0.67, of Cr^{3+} and Nd^{3+} ions contained in these samples, respectively. The differences in the absorption spectra of Nd:Cr:YGAG and Nd:Cr:YAG in Fig. 1 are (i) inhomogeneous broadening of the Nd^{3+} lines in Nd:Cr:YGAG caused by substitution of Ga^{3+} for Al^{3+} and (ii) 5% enhancement of the widths of the $^4T_1(1)$ and $^4T_2$ bands, compared with those in Nd:Cr:YAG.

Figure 2 shows the normalized luminescence spectra excited at 390 nm and 430 nm in the $^4T_1(1)$ absorption band of Cr^{3+} for Nd:Cr:YGAG at 300 K. These spectra consist of intense sharp lines and weak bands around 700 nm and weak sharp lines around 900 nm. Excitation at 430 nm produces two distinct R lines at 689 and 694 nm, whereas that at 390 nm produces the intense R line at 694 nm and the fairly weak R line at 689 nm. Two bands around 678 and 707 nm are phonon-absorbed and phonon-emitted side bands of Cr^{3+}, respectively [9]. The near IR luminescence lines are due to the optical transitions from the metastable $^4F_{3/2}$ excited state of Nd^{3+} to the $^4I_{9/2}$ lowest state [3,8,9]. The peak wavelength (689 nm) of the R line excited at 430 nm for Nd:Cr:YGAG is slightly red-shifted, compared with that (688 nm) for Nd:Cr:YAG [2,8]. The new R line at 694 nm appears only in Nd:Cr:YGAG, but not in Nd:Cr:YAG or Cr:YAG.

Several sharp dips at (676, 685 nm) and (737, 744, 748, 755 nm) in Fig. 2 were observed within these phonon-side bands. The wavelengths of these dips are coincident with the Nd^{3+} absorption lines due to the $^4I_{9/2} \rightarrow {}^4F_{9/2}$, $^4F_{7/2}$ transitions for Nd:YAG as shown in the top of the figure, revealing the Cr^{3+} luminescence is partly reabsorbed by the Nd^{3+} ions. Both excitations at 390 and 430 nm additionally produce weak near IR luminescence lines from the Nd^{3+} ion. The Nd^{3+} luminescence excited at 430 nm is more intense than that at 390 nm. This observation of the Nd^{3+}

luminescence excited in the Cr^{3+} absorption bands indicates energy transfer from Cr^{3+} to Nd^{3+}.

Figure 3(a) shows the temperature dependence of the Cr^{3+} luminescence excited at 390 nm for Nd:Cr:YGAG. The baselines of these spectra are shifted for clarity and the intensities are normalized by their peak intensities. The Cr^{3+} luminescence spectrum with 390 nm excitation at 8 K consists of the R line at 687 nm and the phonon-side bands around 707 and 723 nm. The R line observed at 8 K is labelled as R_1 line because an excited electron of Cr^{3+} is negligibly distributed in an upper level of the orbital-doublet ^2E states at 8 K, of which energy separation is about 20 cm^{-1} [10,11]. However, the line-width is fairly large compared with that in Cr:YAG crystals. Such broadening of the R line is caused by the substitution of Ga^{3+} for Al^{3+}. In increasing temperatures above 100 K, the new R_1 and R_2 lines due to transitions from the doublet ^2E excited states appear at around 692 nm and their intensities at 300 K are comparable with that at 688 nm. This fact suggests that when temperatures increase above 100 K, energy transfer occurs from one Cr^{3+} site associated with the 688 nm R line to another Cr^{3+} site associated with the 692 nm R line. Above 200 K, the phonon-absorbed side band around 678 nm and the background spectrum with a fairly large width clearly appears, and are assigned to anti-Stokes shift band and the transition from the thermally populated $^4T_2$ excited state, respectively. Figure 3(b) shows the temperature dependence of the Cr^{3+} luminescence excited at 430 nm. These spectra are dominantly composed of the 688 nm R line and the phonon-side bands. The behaviour is the same as that in Fig. 3(a) except for the weaker 692 nm R line.

Figure 4 shows the R_1 lines with high resolution and the 390 nm excitation at 8 K for Nd:Cr:YGAG. The R_1 lines are classified into two groups positioned at ~688 and ~693 nm, denoted by numbers (0,1,2,3) and (4), respectively. Dot-dashed curves as a function of wavelength in Fig. 4 are calculated using Gaussian functions with an assumption that variation of wave number as an energy unit is approximately proportional to that of wavelength in a fairly narrow range. The observation of the five R_1 lines deduces distinct Cr^{3+} centers with different crystal fields, being created by the substitution of Ga^{3+}, for example, for octahedral Al^{3+} sites and dodecahedral Y^{3+} sites, respectively. The details will be discussed in the following section.

Figure 5 shows the temperature dependence of the Cr^{3+} and Nd^{3+} luminescence intensities with excitation at 430 nm. The Cr^{3+} luminescence spectrum is decomposed into the ^2E component of the R line and its phonon-side bands, and the $^4T_2$ component as the background. The total intensities of the ^2E and $^4T_2$ components of the Cr^{3+} luminescence are integrated over the range of

640-800 nm as shown in Fig. 2, whereas for the Nd^{3+} luminescence, it is integrated over the range of 860-960 nm. The marked results are as follows; (i) the intensity of the ^2E component of the Cr^{3+} luminescence decreases drastically above 20 K, whereas the $^4T_2$ component increases gradually above 150 K; and (ii) in increasing temperature, the intensity of the Nd^{3+} luminescence also gradually increases, the intensity at 300 K is ~1.5 times larger than at 8 K. The enhancement of the intensity of the $^4T_2$ component is simply represented by the Arrhenius equation. The detailed analyses will be discussed in the following section.

Figure 6 shows the excitation spectra of the R lines at 689 and 694 nm and the Nd^{3+} luminescence line at 885 nm for Nd:Cr:YGAG at 300 K. The excitation spectrum of the Cr^{3+} luminescence at 689 nm is composed of the $^4T_1(1)$ and $^4T_2$ broad bands of the Cr^{3+} ion where each band has double peaks, whereas that of the 694 nm luminescence consists of the $^4T_1(1)$ and $^4T_2$ single broad bands. The latter bands are relatively narrow and blue-shifted, compared with the former bands. The excitation spectrum of the 885 nm luminescence lines of Nd^{3+} is the superposition of the Cr^{3+} absorption bands and the Nd^{3+} absorption lines. The observation of the Cr^{3+} bands in the Nd^{3+} excitation spectrum gives evidence on the energy transfer from Cr^{3+} to Nd^{3+}. The two double-peaked excitation bands of the 689 nm luminescence can be decomposed into two bands using those at 885 and 694 nm, denoted by dotted and dot-dashed lines in Fig. 6, respectively. The result supports the existence of two Cr^{3+} groups, as shown in Fig. 4. The peaks of the $^4T_1(1)$ and $^4T_2$ bands in the excitation spectrum of the 885 nm luminescence in Nd:Cr:YGAG are in agreement with those in Nd:Cr:YAG [8]. The widths of the $^4T_1(1)$ and $^4T_2$ bands are a little enhanced with about 4% and 9%, respectively, compared with those in Nd:Cr:YAG [8]. However, the Cr^{3+} excitation bands of the 694 nm luminescence are blue-shifted so that this new Cr^{3+} center is expected to have a larger crystal field than that for Nd:Cr:YAG [8,9].

In addition, both excitation spectra of the Cr^{3+} luminescence at 689 and 694 nm show several dips around 530 and 580 nm in the $^4T_2$ band of Cr^{3+}. The positions of these dips are completely in agreement with the peak wavelengths of the Nd^{3+} absorption lines for Nd:YAG due to the optical transitions from the $^4I_{9/2}$ ground state to the $^4G_{7/2}$ and $^4G_{5/2}$ excited states, as shown in the top of Fig. 6. Such dips around 530 and 580 nm may be produced by reduction of the Cr^{3+} luminescence through the simultaneous sharp Nd^{3+} absorption overlapping with the Cr^{3+} absorption band as shown in Fig.1.

Figure 7 shows the decay curves of the 689 and 694 nm luminescence of the Cr^{3+} ion with

various excitation wavelengths for Nd:Cr:YGAG at (a) 2.5 K and (b) 300 K. The decay curve of the 688 nm R line for Cr:YAG observed at 300 K is added for comparison purpose. The decay curve of the 689 nm luminescence at 2.5 K is very similar to that of the 694 nm luminescence, because the 694 nm R line excited at 390 nm is hardly observed at 8 K as shown in Fig. 3(a) and the dominant luminescence intensity at 694 nm is due to the phonon-side band of the 689 nm R line. The decay curves of the 689 nm R line excited at 451 and 633 nm, and the 694 nm R line excited at 370 nm at 300 K as shown in Fig. 7(b) is represented by multi-exponential functions. Markedly, the dominant slow component of the 694 nm R line gives a decay time of 2.8 ms, that is, longer than the 1.7 ms observed for Cr:YAG. The changes in the decay rate of the lowest excited state of Cr^{3+}, when compare to the intrinsic radiative decay rate of Cr^{3+} in YAG, indicate the efficiency of the energy transfer process between the Cr^{3+} ions and the Nd^{3+} ions. The larger the negative difference, the more efficient the energy transfer process.

The analyses of the decay curve including the energy transfer were developed by Inokuchi and Harayama [12]. Their theory is based on energy transfer rates that are strongly dependent on separation distances between sensitizers and activators, leading to a continuous distribution of the decay rate of the luminescence emitted from the sensitizers. In the previous paper [8], the decay curves of the Nd^{3+} and Cr^{3+} luminescence in YAG ceramics were simply decomposed into temperature-independent and temperature-dependent components. The former or latter component corresponds to energy transfer from a Cr^{3+} ion positioned at the origin to a Nd^{3+} ion substituting for one of the first nearest neighbour yttrium dodecahedral sites, or near yttrium ions beyond within a sphere with an approximate radius of less than 0.8 nm, respectively [8]. However, the calculation of the decay rate of the Cr^{3+} luminescence in substitutional disorder crystal, Nd:Cr:YGAG, includes both distributions of the Cr^{3+}-Nd^{3+} distance and the Cr^{3+}-Ga^{3+} distance, so that the energy transfer theory becomes more complicated. As a consequence, it is very difficult to apply the Inokuchi-Harayama's theory to substitutional disordered crystals including such distributions.

In order to simplify such relaxation processes, including the above both distributions, the decay curves are assumed to be approximately decomposed into, at least, three components [8,13], and the origins of three components are deduced, taking accounts of the distributions. The decay curve is given by

$$I(t) = I_1 \times \exp\left(-\frac{t}{\tau_1}\right) + I_2 \times \exp\left(-\frac{t}{\tau_2}\right) + I_3 \times \exp\left(-\frac{t}{\tau_3}\right) \qquad (1)$$

where τ_i (i=1, 2, 3) is a decay time, and I_i (i =1, 2, 3) is an initial intensity at t = 0.

The decay curves of the 689 and 694 nm at 2.5 K in Fig. 7(a) fit to solid lines calculated using Eq. (1) with fitting parameters of (τ_1(ms), τ_2(ms), τ_3(ms))=(0, 1.95, 5.5) and (0, 1.95, 6.0), respectively. Their parameters are very close to each other except for their initial intensity. The fitting parameters (τ_1(ms), τ_2(ms), τ_3(ms)) of the decay curves with (λ_{ex}(nm), λ_{em}(nm)) =(451, 689), (633, 689), and (370, 694) at 300 K as shown in Fig. 7(b) are also given by (0.13, 0.58, 2.2), (0.11, 0.35, 0.76) and (0.13, 0.54, 2.8), respectively. In comparison, the decay curve of the 688 nm R line excited at 633 nm for Cr:YAG fits well to a single exponential function with the decay time of 1.7 ms.

Decay curves of the R lines at 689 nm for Nd:Cr:YGAG and at 688 nm for Cr:YAG were measured at several excitation wavelengths in the $^4T_1(1)$ and $^4T_2$ absorption bands of the Cr^{3+} ion at 300 K. Figure 8 shows the decay times as a function of excitation wavelength for Nd:Cr:YGAG and Cr:YAG. The three decay times, τ_1, τ_2, τ_3, for Nd:Cr:YGAG are denoted by open circles and that for Cr:YAG is denoted by solid circles. The decay time (1.7 ms) for Cr:YAG is independent of the excitation wavelengths. The decay times, τ_1, τ_2, for Nd:Cr:YGAG are shorter than that for Cr:YAG, whereas τ_3 is longer than that for Cr:YAG except for the 633 nm excitation. The decay times are shortened at each $^4T_1(1)$ or $^4T_2$ absorption band tail at ~450 and ~630 nm, respectively. The large reduction of the decay times from that of Cr:YAG is due to both distributions of distances between Cr^{3+} and Nd^{3+} and between Cr^{3+} and Ga^{3+}, namely, the distributions of the energy transfer rate and the Cr^{3+} crystal field strength. The details will be discussed in the following section.

Figure 9 shows the temperature dependence of the decay times of the Cr^{3+} luminescence at 689 nm and 694 nm excited at 451 nm and 370 nm, respectively, in the temperature range of 2.5-300 K. Although the decay curves below 30 K fit to two exponential functions, the same as in Fig. 7(a), the curve fitting above 30 K requires, at least, three exponential functions. The decay times of the three decomposed components decreased gradually with an increasing temperature. The three decay components of the 694 nm luminescence excited at 370 nm below 150 K are almost in agreement with those of the 689 nm luminescence with the 451 nm excitation. This result is

consistent with that of Fig. 3(a), where the 694 nm R line with the 390 nm excitation is very weak below 100 K. However, when the temperature increases above 150 K, their decay times can be distinguished. The longer decay time τ_3 (2.8 ms) of the 694 nm R line at 300 K corresponds to Cr^{3+} centers (number 4) with no energy transfer from Cr^{3+} to Nd^{3+}.

Figure 10 shows the quantum yields of the Nd^{3+} and Cr^{3+} luminescence measured at 300 K with the excitation range of 370-690 nm for Nd:Cr:YGAG, being denoted by open and solid circles, respectively. Here, the Nd^{3+} quantum yield is calibrated using the observed Stark branching ratio (0.3 : 0.56 : 0.14 : 0.01) of the optical transition from $^4F_{3/2}$ to ^4I_J (J = 9/2, 11/2, 13/2, 15/2) of Nd^{3+} in YAG at room temperature, respectively [14]. The Nd^{3+} quantum yield (26%) with the Cr^{3+} excitation for Nd:Cr:YGAG is almost equal to that (22%) with the direct Nd^{3+} excitation (808 nm) for the same crystal. In the case of Nd:YAG, the value of the quantum yield of the Nd^{3+} luminescence excited at 807 nm is 54%. The Nd^{3+} quantum yield of Nd:Cr:YGAG is 0.4 times lower than that of Nd:YAG. The large reduction of the Nd^{3+} quantum yields for Nd:Cr:YGAG suggests poor quality of the YGAG single crystal. This is primarily due to lattice distortion in the Nd:Cr:YGAG crystal as the result of the substitution of Ga^{3+} for Al^{3+} or Y^{3+} ions.

On the other hand, the quantum yields for the Cr^{3+} ion in Nd:Cr:YGAG and Cr:YAG are 7% and 88% , respectively. The large reduction of the Cr^{3+} quantum yield suggests an efficient energy transfer from Cr^{3+} to Nd^{3+}. A shallow dip at 510 nm and decreases below 380 nm and above 670 nm in Fig. 10 correspond to the valley and the tails of the $^4T_1(1)$ and $^4T_2$ bands in Fig. 1. Such decreases may be due to low resolution of an equipment or loss of light scattering in a limited case of the weaker absorption and the weaker emission. Thus, the Cr^{3+} and Nd^{3+} quantum yields may be approximately independent of the wavelengths of the $^4T_1(1)$ and $^4T_2$ absorption bands.

4. Discussion

The basic requirement for solar-pumped laser operation using Nd^{3+} and Cr^{3+} codoped garnet crystals are (i) laser materials absorb efficiently the solar energy in the visible and near IR ranges; and (ii) energy transfer from Cr^{3+} to Nd^{3+} occurs efficiently. Substitutional disordered garnet crystals possess a possibility to match the above requirements. We discuss these points below.

4.1. Substitution of Ga^{3+} and inhomogeneous broadening of Cr^{3+} and Nd^{3+} optical spectra

The $^4T_1(1)$, $^4T_1(2)$, and $^4T_2$ excited states of Cr^{3+} strongly interact with phonons so that the optical transitions to these excited states form broad band structure in the visible range. The full widths at half maximum (W) of the $^4T_1(1)$ and $^4T_2$ absorption bands (energy unit : cm^{-1}) for Nd:Cr:YGAG and Nd:Cr:YAG are estimated to be $(W(^4T_1(1)), W(^4T_2))$=(3400, 2150) and (3250, 2090), respectively. The $^4T_1(1)$ and $^4T_2$ absorption coefficients integrated over the wavelength (A) are calculated to be $(A(^4T_1(1)), A(^4T_2))$= (1663, 1207) and (673, 451) for Nd:Cr:YGAG and Nd:Cr:YAG, respectively. The former indicates that the W value for Nd:Cr:YGAG is 5% larger than that for Nd:Cr:YAG. The latter estimates that the ratio of the integrated $^4T_1(1)$ ($^4T_2$) absorption coefficients of Nd:Cr:YGAG to Nd:Cr:YAG is 2.5 (2.7) and ~10% (~20%) with an experimental error of $\pm$5% larger than the ratio, 2.2, of the Cr^{3+} concentration of Nd:Cr:YGAG to Nd:Cr:YAG. These results suggest that the substitution of Ga^{3+} for Al^{3+} produces inhomogeneous broadening of the Cr^{3+} optical absorption bands, and slightly breaks the selection rule on the parity-forbidden 3d-3d transitions of the Cr^{3+} ion.

Such substitution also produces a distribution of the crystal field strength of the Cr^{3+} ions. Figure 4 shows the existence of various R lines corresponding to the discrete Cr^{3+} crystal fields. These R_1 lines in Fig. 4 are classified into two groups, number (0-3) and number (4). These two groups are associated with the substitution of Ga^{3+} for two different lattice sites. Although Ga^{3+} ions prefer to occupy Al^{3+} octahedral sites, they could also substitute for Y^{3+} ions in dodecahedral sites.

We consider the origin of the first group (number 0-3) of the Cr^{3+} ion. We assume that Cr^{3+} and Ga^{3+} ions substitute preferentially for the octahedral Al^{3+} ions and that Ga^{3+} ions occupy the first nearest neighbor octahedral sites with the Cr^{3+} ion positioned at the origin. There are eight equivalent first nearest neighbor Al^{3+} sites. The formation probability, P_n, of complex $CrGa_nAl_{8-n}$ including the first nearest neighbors composed of nGa and (8-n)Al are calculated by

$$P_n = {}_8C_n c^n (1-c)^{8-c} \qquad (2)$$

where c is the probability that a Ga^{3+} ion occupies an octahedral Al^{3+} site and $\sum_{n=0}^{8} P_n = 1$. The ratio of $P_0 : P_1 : P_2 : P_3 : P_4 : P_5 : P_6 : P_7 : P_8$ is calculated to be 0.39 : 0.39 : 0.17 : 0.04 :~ 0 : ~0 : ~0 : ~0 using Eq. (2) and c=0.11 estimated from the composition of $Y_{2.97}Nd_{0.02}Ga_{0.22}Al_{4.68}Cr_{0.11}O_{12}$.

The integrated intensity ratio for the observed R_1 lines numbered 0, 1, 2, and 3 in Fig. 4 was 0.21 : 0.48 : 0.22 : 0.09. The observed ratio is very close to the calculated one.

Let's consider the second group of numbered 4 corresponding to the 694 nm R lines. A jump from 689 nm to 694 nm cannot be explained by the substitution of Ga^{3+} for the octahedral Al^{3+} ions. A possible model is proposed that a Ga^{3+} ion substitutes for a dodecahedral Y^{3+} ion. Such substitution may produce a large Cr^{3+} crystal field through the lattice compression because the ionic radius of Ga^{3+} is smaller than that of Y^{3+} [14]. This is consistent with the Cr^{3+} higher crystal field corresponding to the 694 nm R lines, that is, the blue-shift of the $^4T_1(1)$ and $^4T_2$ excitation bands as shown in Fig. 6.

This substitution also affects the Cr^{3+} crystal field, which determines not only energy levels of the $^4T_1$ (1) and $^4T_2$ excited states, but also the decay rate from the ^2E lowest excited state. In the following subsection, the decay process is discussed, including energy transfer from Cr^{3+} to Nd^{3+}.

4.2. Energy transfer from Cr^{3+} to Nd^{3+}

We consider a single Cr-Nd pair with a fixed separation distance R without a distribution of the Cr^{3+} crystal field. The observed decay time (τ'_{Cr}) of the luminescence from a Cr^{3+} center in Nd:Cr:YGAG is given by,

$$\frac{1}{\tau'_{\mathrm{Cr}}} = \frac{1}{\tau_{\mathrm{Cr}}} + \frac{1}{\tau_{tr}} \ , \qquad (3)$$

where $1/\tau_{tr}$ is an energy transfer rate from Cr^{3+} to Nd^{3+}, and $1/\tau_{\mathrm{Cr}}$ is the decay rate of the intrinsic Cr^{3+} luminescence [3,8,9].

The energy transfer rate, $1/\tau_{\mathrm{tr}}$, in Eq. (3) can be represented by a power function of R,

$$\frac{1}{\tau_{tr}} = \frac{\beta^{(n)}}{R^n} \quad n = 6, 8, 10, \qquad (4)$$

where $\beta^{(n)}$ is the microscopic interaction parameter between Cr^{3+} and Nd^{3+} ions of the pair, and n has the value of 6, 8, or 10, for dipole-dipole, dipole-quadrupole, or quadrupole-quadrupole interaction mechanisms, respectively [3,9,12]. When the separation distances are distributed, the

energy transfer rates also distribute. Inokuti and Hirayama formulated the rates assuming an uniform distribution of the sensitizers and activators in materials [12].

The decay rates ($1/\tau_{\mathrm{Cr}}$) of the intrinsic Cr^{3+} luminescence in Cr:YAG and Cr:YGAG without Nd^{3+} ions as a function of temperature, T, are formulated in the form of [3,8,9],

$$\frac{1}{\tau_{\mathrm{Cr}}} = \frac{\frac{1}{\tau_{\mathrm{E}}}+\frac{1}{\tau_{\mathrm{T}}}\exp\left(-\frac{\Delta}{k_B T}\right)}{1+\exp\left(-\frac{\Delta}{k_B T}\right)} \tag{5}$$

where τ_{E} and τ_{T} are the intrinsic decay times from the ^2E and $^4T_2$ excited states of Cr^{3+} to the $^4A_2$ ground state, respectively, and Δ is the energy separation between the ^2E and $^4T_2$ excited states. The values of τ_{E}, τ_{T} and Δ in Cr:YAG were obtained to be 8 ms, 23 μs and 945 cm^{-1} from the temperature dependence of the decay times, respectively [8]. The intensities of the decomposed ^2E and $^4T_2$ components of the Cr^{3+} luminescence proportional to the decay rate of each component of ^2E or $^4T_2$ in Eq. (5) are given by [15,16],

$$I_{\mathrm{E}} = \frac{I_0}{1+\exp\left(-\frac{\Delta}{k_B T}\right)} \tag{6}$$

$$I_{\mathrm{T}} = \frac{I_0\left(\frac{\tau_{\mathrm{E}}}{\tau_{\mathrm{T}}}\right)\exp\left(-\frac{\Delta}{k_B T}\right)}{1+\exp\left(-\frac{\Delta}{k_B T}\right)} \quad . \tag{7}$$

The $^4T_2$ component of the Cr^{3+} luminescence intensity in Nd:Cr:YGAG calculated using Eq. (7) and the energy separation of Δ=630 cm^{-1}, fits well to the observed integrated intensities of the $^4T_2$ component in Fig. 5 (a). The result that the energy separation of Δ=630 cm^{-1} for Nd:Cr:YGAG is smaller than that (945 cm^{-1}) in Cr:YAG implies a decrease of the Cr^{3+} crystal field strength. Next, τ_{Cr} in Eq. (5) is calculated to be ~0.5 ms using the parameters of τ_{E}(=8 ms), τ_{T}(=23 μs), Δ(=630 cm^{-1}) and T(= 300 K). This calculation is very close to that (0.4-0.6 ms) of τ_2 for Nd:Cr:YGAG at 300 K observed in Figs. 8 and 9 and larger than that (0.1-0.16 ms) of τ_1. This result suggests that first approximation of the decay rate is given by the distribution of the Cr^{3+}

crystal field, followed by the energy transfer.

Let's consider the faster decay rate, $1/\tau_1$. The difference in the decay rates of $1/\tau'_{\mathrm{Cr}}$ (=$1/\tau_1$) and $1/\tau_{\mathrm{Cr}}$ in Nd:Cr:YGAG is equal to the energy transfer rate, $1/\tau_{tr}$, in Eq. (4). The ratio of $1/\tau_{tr}$ to $1/\tau_{\mathrm{Cr}}$ at room temperature is roughly estimated to be ~3:1. This calculation suggests that approximate 75 % amount of the fast component in the Cr^{3+} decay curve is associated with the energy transfer to Nd^{3+}.

On the other hand, the decay time (~2.8 ms) of the 694 nm R line at 300 K is larger than that (1.7 ms) of the 688 nm R line at 300 K for Cr:YAG. This fact suggests that the decay rate includes neither the energy transfer term in Eq. (3) nor the contribution of the $^4T_2$ excited state in Eq. (5) because the separation energy is expected to be larger than that (945 cm^{-1}) of YAG.

Finally, we discuss the rapid decrease of the ^2E intensity of the Cr^{3+} luminescence above 20 K. The temperature dependence of the ^2E component calculated using Eq. (6) with Δ=100 cm^{-1} fits well to the observed measurement in Fig. 5(a). The calculated value (Δ=100 cm^{-1}) is fairly smaller than that (Δ=630 cm^{-1}) estimated for the $^4T_2$ component in Fig. 5(a). This result suggests that the excited electron of the lowest ^2E excited state at low temperatures relaxes not through the $^4T_2$ higher excited state, but to the higher ^2E vibronic state, lying about 100 cm^{-1} above the ^2E zero-phonon energy level. The vibronic energy level of Cr^{3+} is completely coincident with that the $^4F_{9/2}$ multiplet of Nd^{3+} as shown in Fig. 2. The enhancement of the Nd^{3+} luminescence occurs through the energy transfer via this vibronic energy level of Cr^{3+}. Furthermore, the Nd^{3+} luminescence intensity increased gradually with increasing temperature above 150 K as shown in Fig. 5(b). Such additional enhancement occurs through another energy transfer path via thermal population of the $^4T_2$ excited state of Cr^{3+}.

4.3. Quantum yields of Cr^{3+} and Nd^{3+} luminescence

The quantum yields of the Nd^{3+} luminescence excited at 430 and 808 nm for Nd:Cr:YGAG are obtained to be 24% and 22%, respectively, whereas that of the Nd^{3+} luminescence excited at 808 nm for Nd:YAG is 54%. The large reduction of the quantum yields of the Nd^{3+} luminescence from 54% to 22% may be due to degradation of the YGAG crystalline quality. On the other hand, the quantum yields of the Cr^{3+} luminescence excited at 430 nm for Nd:Cr:YGAG and Cr:YAG are 7% and 88%, respectively. Assuming that the extent of the YGAG crystalline degradation is equal to the ratio of ~0.4 of the Nd^{3+} quantum yield for Nd:Cr:YGAG to that for Nd:YAG, the

reduction of the Cr^{3+} quantum yield from 88% to 7% for Nd:Cr:YGAG deduces that about 80% of Cr^{3+} transfers resonantly to Nd^{3+}. This value is nearly equal to that (75%) estimated from the decay rate ($1/\tau_1$) of the fast component in the Cr^{3+} decay curve observed for Nd:Cr:YGAG.

5. Conclusions

The $T_1(1)$ and $^4T_2$ optical absorption bands of Cr^{3+} in Nd:Cr:YGAG are broadened by the electron-phonon interaction. The substitution of 5% Ga^{3+} ions to Al^{3+} ions in the YGAG crystal further causes inhomogeneous broadening of the Cr^{3+} absorption bands. The enhancement of their band widths is about 5%. A further increase of the Ga concentration leads to not only larger inhomogeneous broadening of the Nd^{3+} and Cr^{3+} absorption spectra, but also the degradation of the crystalline quality. In order to apply the substitutional disordered garnet crystals to the solar-pumping laser system, it is required to optimize the Ga concentration or seek other suitable substitutional elements, for example, Lu or Gd for Y and Sc for Al.

Acknowledgment

This work was supported by the Use-of-UVSOR Facility Program (26-808) of the Institute for Molecular Science.

References

[1] W. Koechner, Solid-State Laser Engineering, Springer-Verlag, Berlin, 1996, Chap. 2.

[2] P. Hong, X. X. Zhang, C. W. Struck, B. Di Bartolo, J. Appl. Phys. **78** (1995) 4659-4667.

[3] R. C. Powell, Physics of Solid-State Laser Materials, Springer-Verlag, New York, 1998, Chaps. 5 and 8.

[4] G. Armagan, B. Di Bartolo, in Tunable Solid-State Lasers Ⅱ, edited by A. B. Budgor, L. Esterowitz, L. G. DeShazer, Springer-Verlag, Berlin, 1986, pp. 35-43.

[5] V. G. Ostroumov, Yu. S. Privis, V. A. Smirnov, I. A. Shcherbakov, J. Opt. Soc. Am. **B 3** (1986) 81-93.

[6] A. A. Silva-Moreno, M. A. M. Nava, O. Barbosa-Garcia, L. A. Diaz-Torres, F. C. Romo, G. Boulon, Opt. Master. **16** (2001) 221-226.

[7] M. Zokai, R. C. Powell, G. F. Imbusch, B. Di Bartolo, J. Appl. Phys. **50** (1979) 5930-5936.

[8] M. Yamaga, Y. Oda, H. Uno, K. Hasegawa, H. Ito, S. Mizuno, J. Appl. Phys. **112** (2012) 063508-1-12.

[9] B. Henderson, G.F. Imbusch, Optical Spectroscopy of Inorganic Solids, Clarendon Press, Oxford, 1989, Chaps. 5 and 8.

[10] K.P. O'Donnell, A. Marshall, M. Yamaga, B. Henderson, B. Cockayne, J. Lumin. **42** (1989) 365-373.

[11] M. Erdem, G. Ozen, U. Yahsi, B. Di Bartolo, J. Lumin. **158** (2015) 464-468.

[12] M. Inokuti, F. Hirayama, J. Chem. Phys. **43** (1965) 1978-1989.

[13] M. Yamaga, H. Uno, S. Tsuda, J.-P. R. Wells, T. P. J. Han, J. Lumin. **132** (2012) 1608-1617.

[14] A. A. Kaminski, Laser Crystals, Springer-Verlag, Berlin, 1990, Chap.6.

[15] M. Yamaga, B. Henderson, K.P. O'Donnell, C.T. Cowan, A. Marshall, Appl. Phys. **B50** (1990) 424-431.

[16] M. Yamaga, B. Henderson, K.P. O'Donnell, G. Yue, Appl. Phys. **B51** (1990) 132-136.

Figure captions

Fig. 1. Absorption spectra observed for Nd:Cr:YGAG and Nd:Cr:YAG at 300 K. The base line for Nd:Cr:YGAG is shifted for clarity.

Fig. 2. Luminescence spectra of Cr^{3+} and Nd^{3+} excited at 390 nm and 430 nm for Nd:Cr:YGAG at 300 K. Spectra are normalized by the maximum intensities. Top of the figure is the absorption spectrum for Nd:YAG.

Fig. 3. Temperature dependence of the Cr^{3+} luminescence spectra for Nd:Cr:YGAG excited at (a) 390 nm and (b) 430 nm.

Fig. 4. R_1 lines with high resolution and 390 nm excitation at 8 K for Nd:Cr:YGAG. The dot-dashed lines numbered 0-3 are calculated using four Gaussians.

Fig. 5. Temperature dependence of integrated intensities of (a) the Cr^{3+} luminescence composed of the ^2E and $^4T_2$ components, and (b) the Nd^{3+} luminescence intensities with the 430 nm excitation.

Fig. 6. Excitation spectra of the Cr^{3+} luminescence at 689 nm and 694 nm and the Nd^{3+} luminescence at 885 nm in Nd:Cr:YGAG at 300 K. All spectra are normalized by the maximum intensities. Top of the figure is the absorption spectrum for Nd:YAG.

Fig. 7. Decay curves of the 689 and 694 nm luminescence of Cr^{3+} excited at 370, 451 and 633 nm for Nd:Cr:YGAG at (a) 2.5 K and (b) 300 K, compared with that excited at 633 nm for Cr:YAG. Solid lines are calculated using Eq. (1) and fitting parameters in the text.

Fig. 8. Three decay times (τ_1, τ_2, τ_3) of the 689 nm luminescence of Cr^{3+} in Nd:Cr:YGAG and the 688 nm luminescence of Cr^{3+} in Cr:YAG as a function of excitation wavelength at 300 K, being denoted by open and solid circles, respectively.

Fig. 9. Temperature dependence of three decay times (τ_1, τ_2, τ_3) of the Cr^{3+} luminescence at 689 nm and 694 nm excited at 451 nm and 370 nm.

Fig. 10. Quantum yields of the Nd^{3+} and Cr^{3+} luminescence for Nd:Cr:YGAG at 300K as a function of excitation wavelength, being denoted by open and solid circles, respectively.

Fig. 1

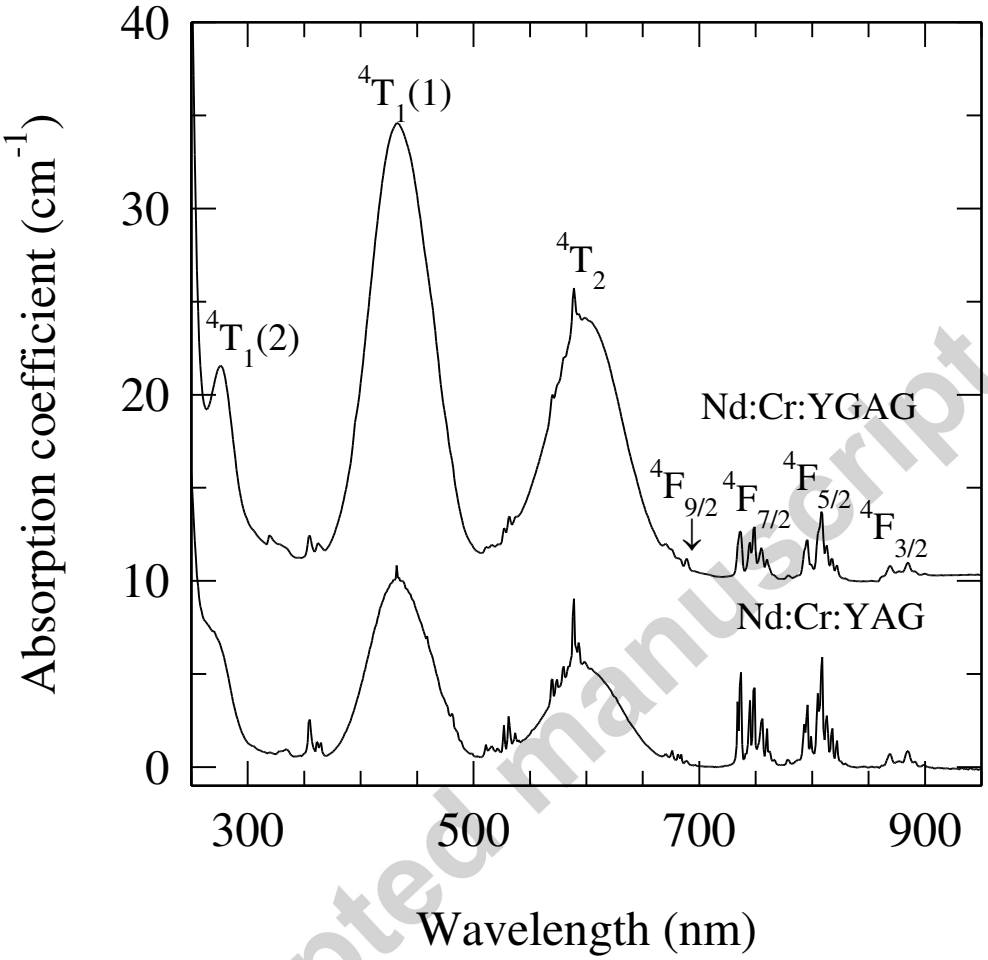

Fig. 2

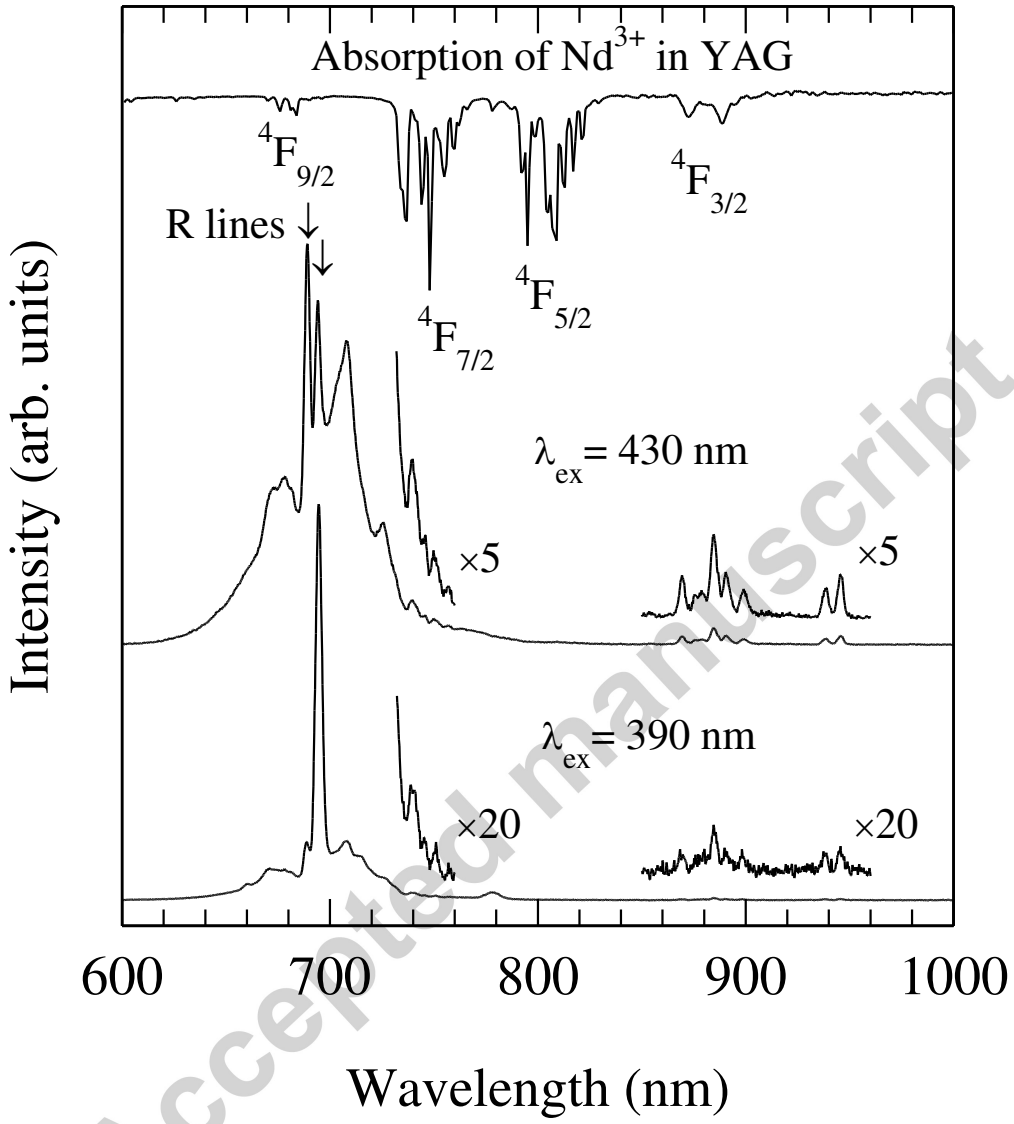

Fig. 3

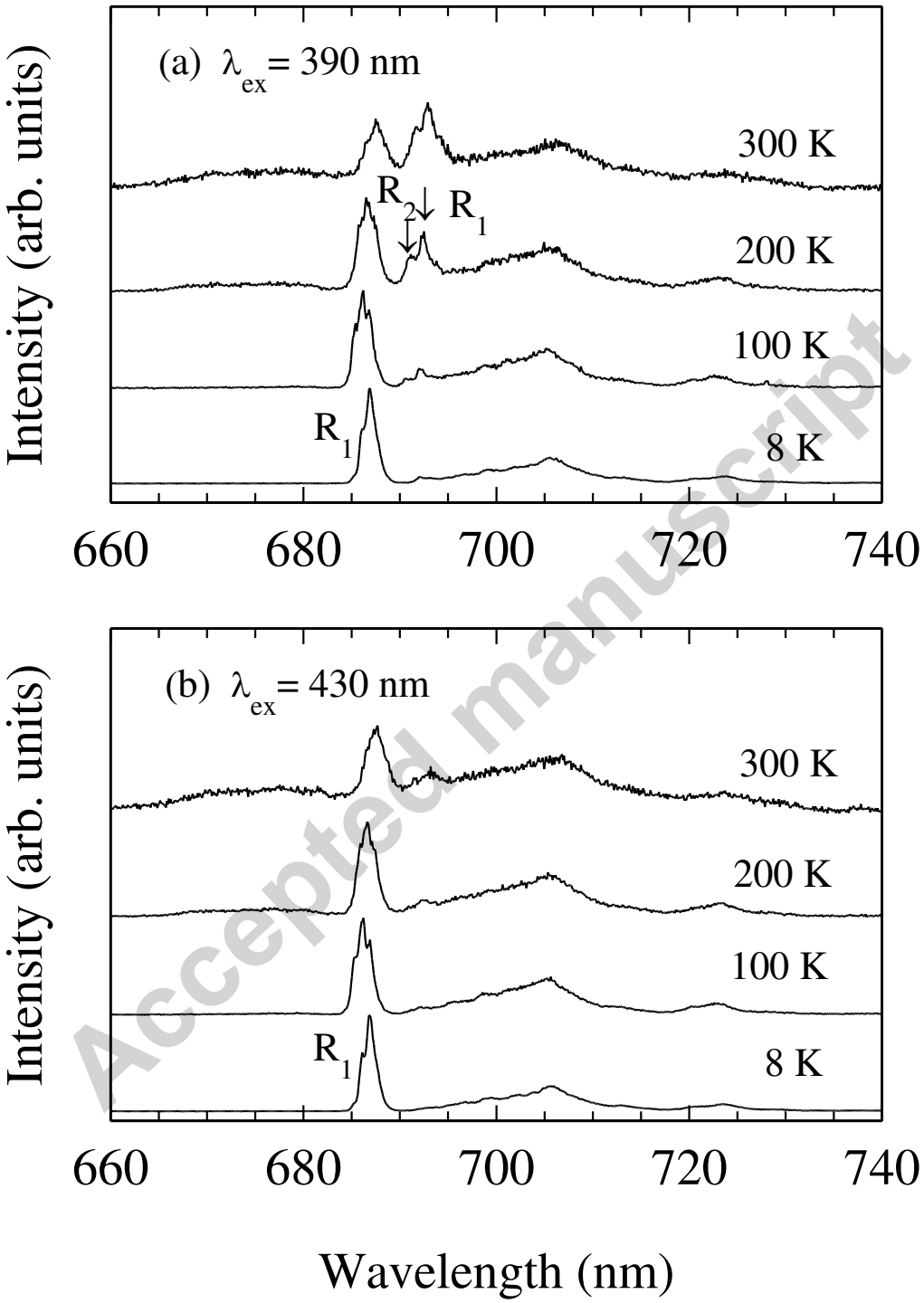

Fig. 4

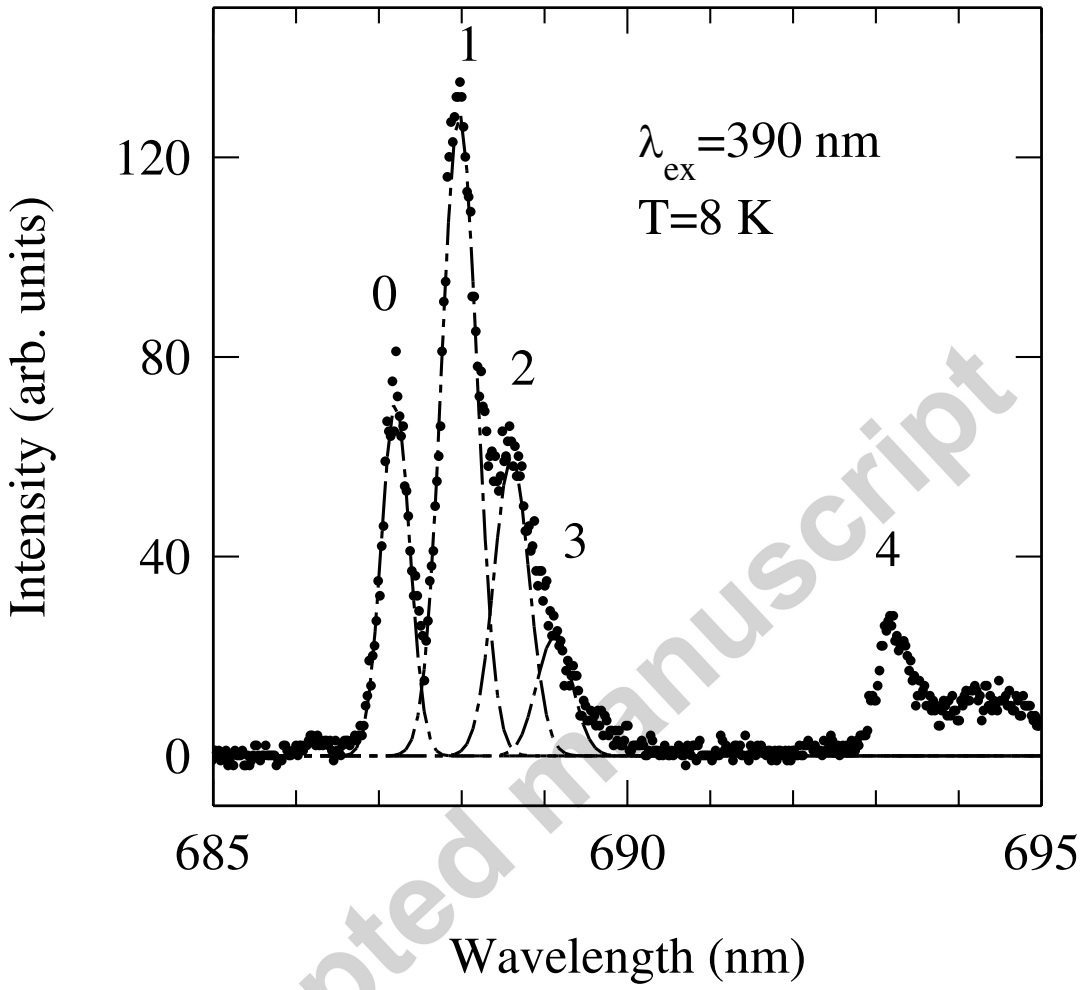

Fig. 5

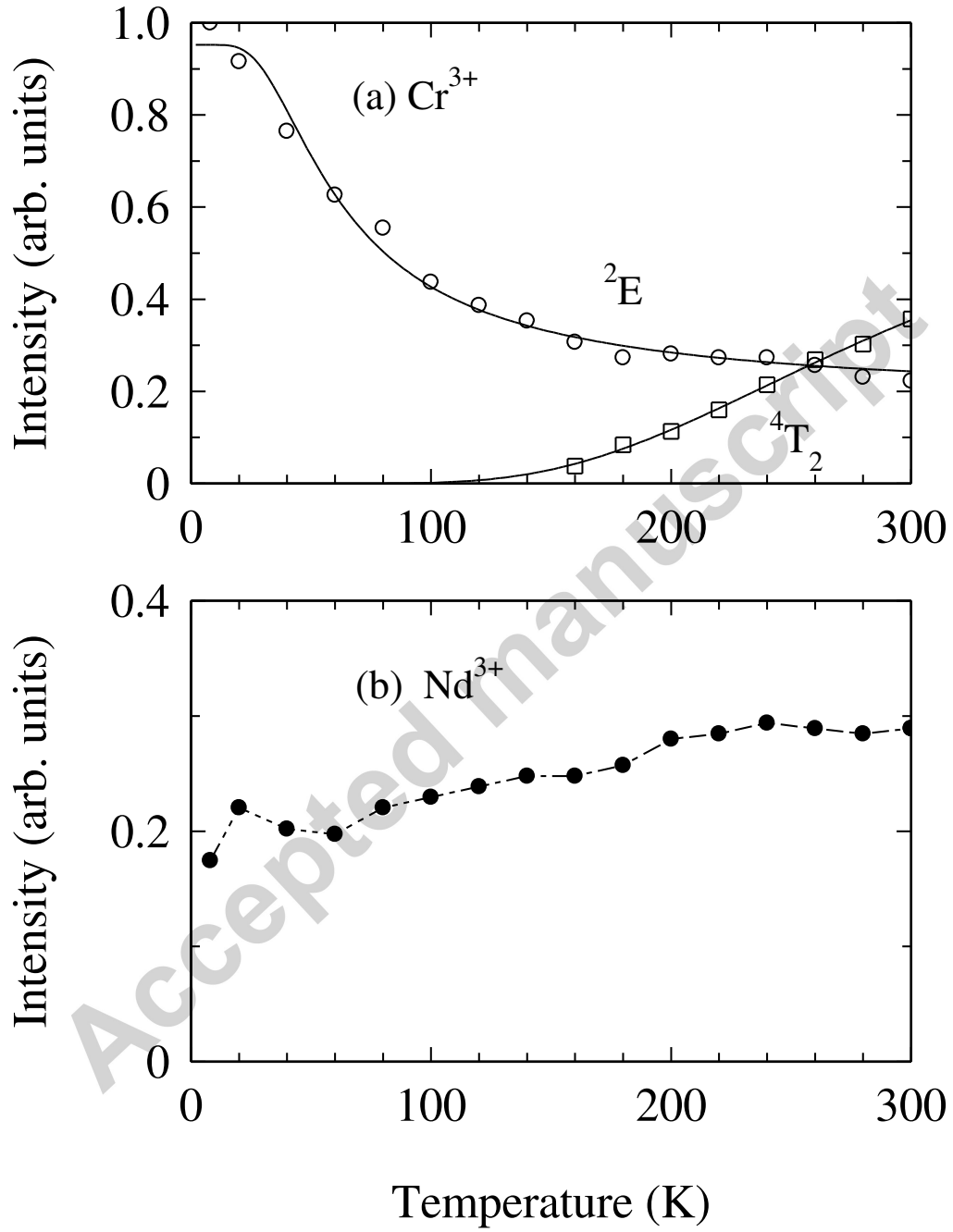

Fig. 6

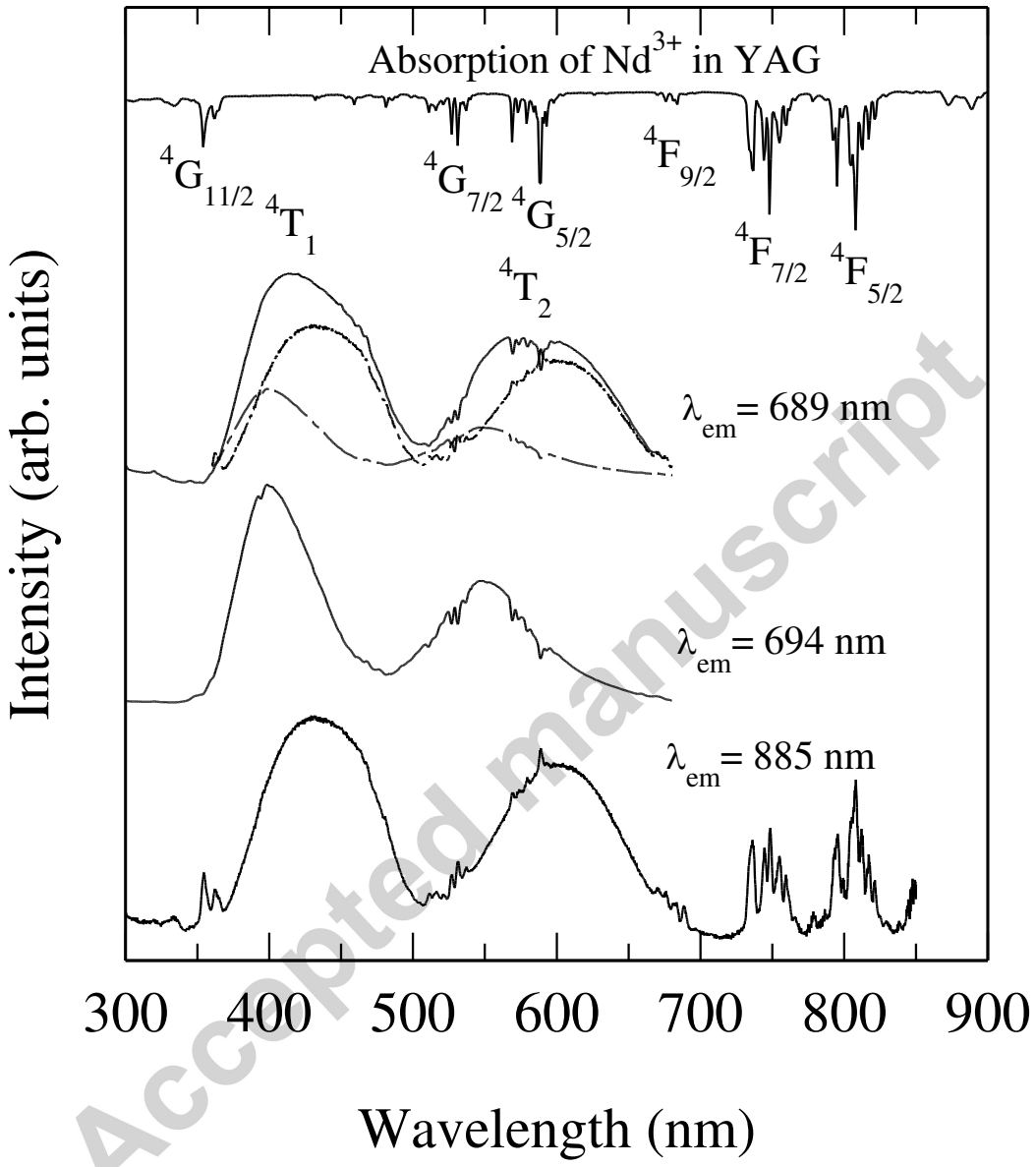

Fig. 7

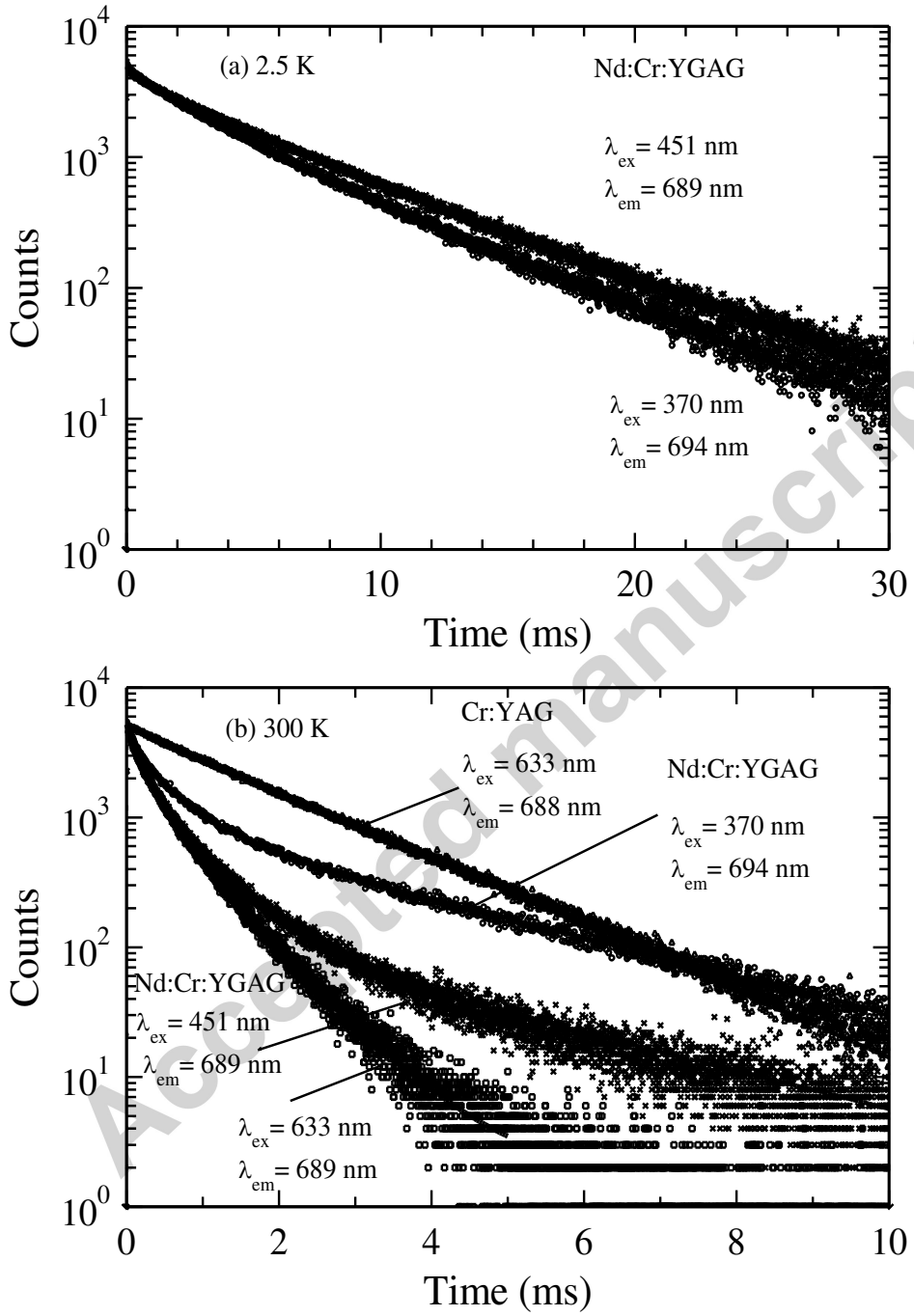

Fig. 8

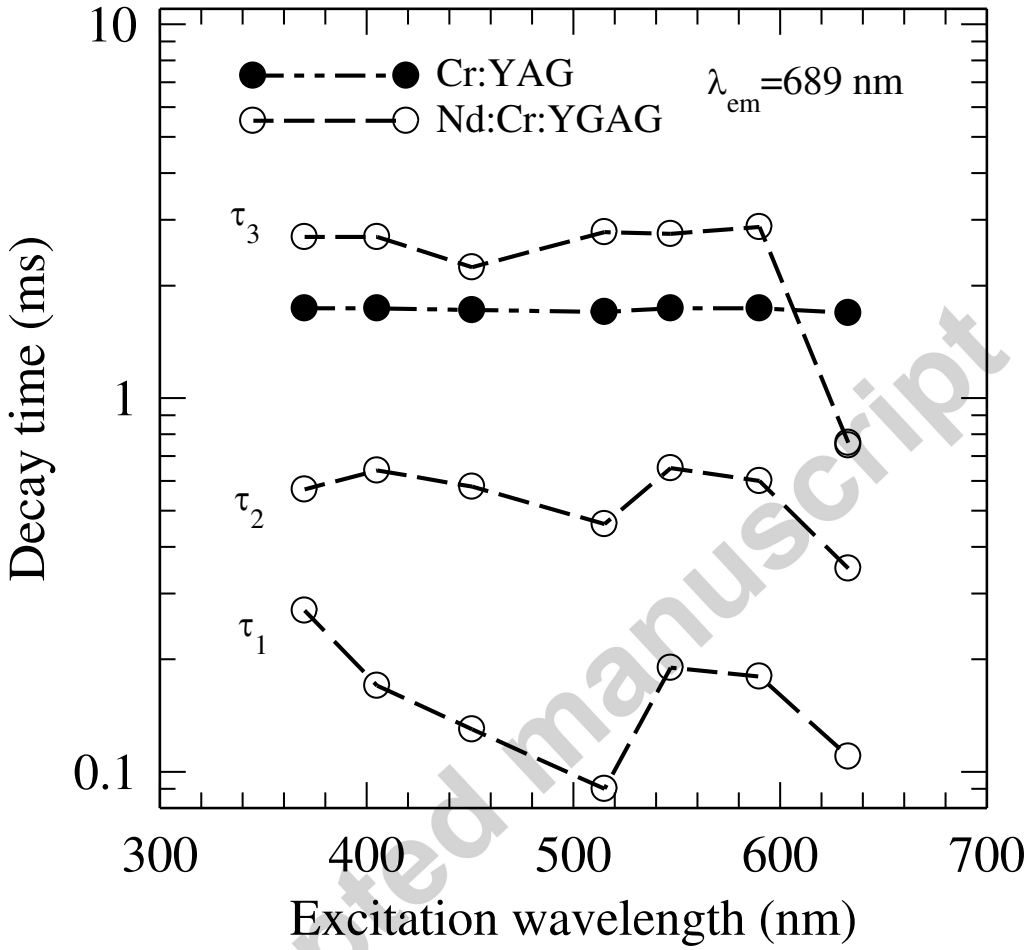

Fig. 9

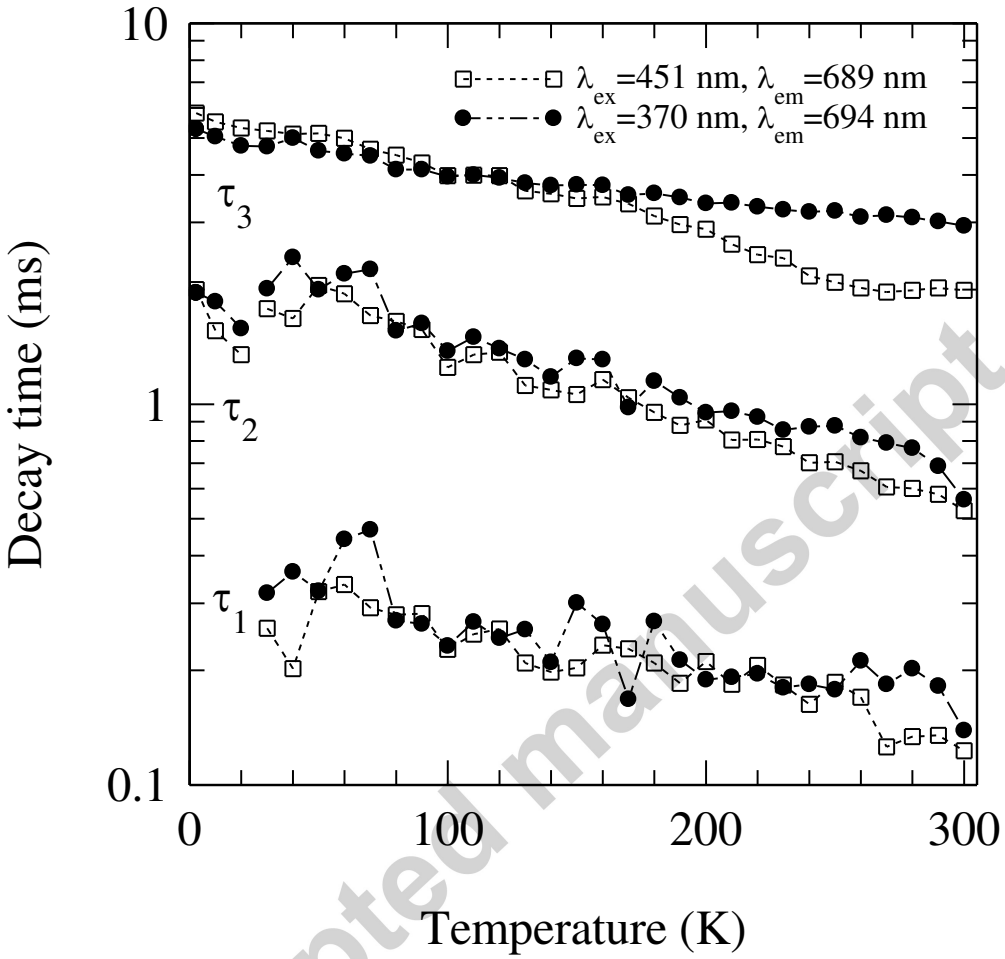

Fig. 10

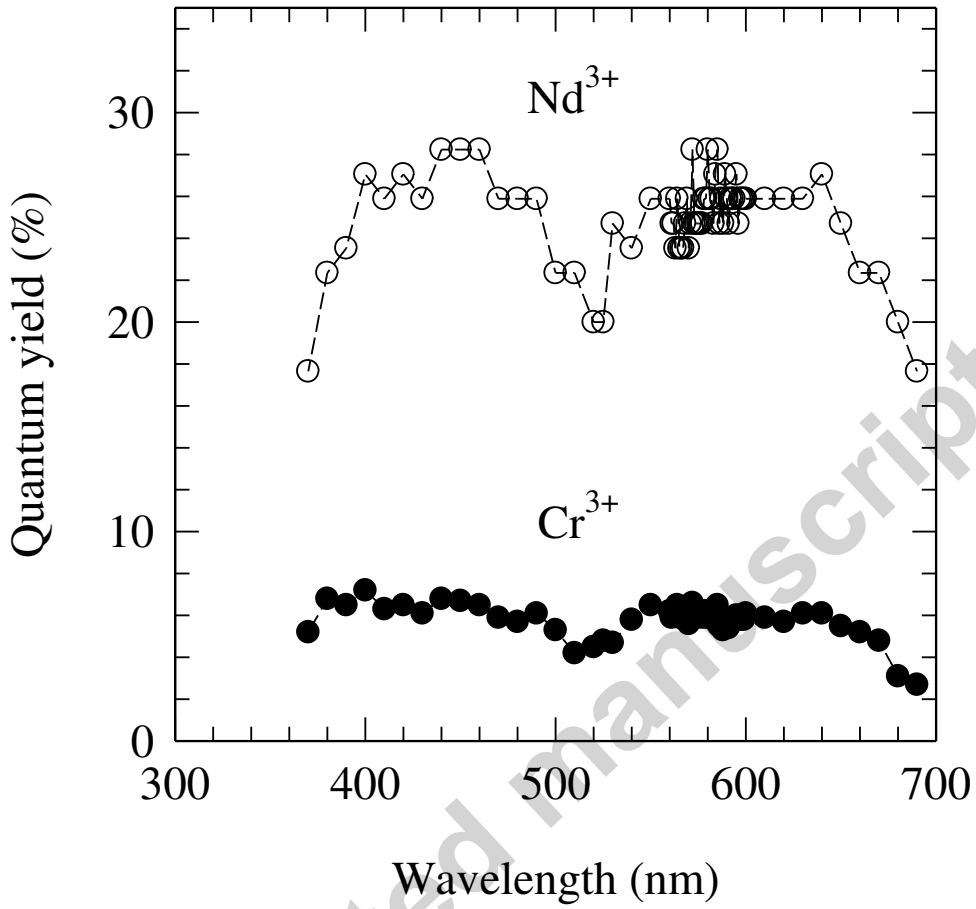

Highlights

1. Substitutional disordered garnet crystals $Y_3Ga_xAl_{5-x}O_{12}$ codoped with Nd^{3+} and Cr^{3+} ions are candidates of solar-pumped laser materials.
2. The substitution produces inhomogeneous broadening of the Nd^{3+} and Cr^{3+} optical spectra.
3. Inhomogeneous broadening of the Cr^{3+} absorption bands and energy transfer from Cr^{3+} to Nd^{3+} enhance the solar-pumping efficiency of Nd^{3+}.